

Size effect on splitting strength of hardened cement paste: Experimental and numerical study

Zhang, Hongzhi; Šavija, Branko; Xu, Yading; Schlangen, E.

DOI

[10.1016/j.cemconcomp.2018.09.018](https://doi.org/10.1016/j.cemconcomp.2018.09.018)

Publication date

2018

Document Version

Final published version

Published in

Cement and Concrete Composites

Citation (APA)

Zhang, H., Šavija, B., Xu, Y., & Schlangen, E. (2018). Size effect on splitting strength of hardened cement paste: Experimental and numerical study. *Cement and Concrete Composites*, 94, 264-276. <https://doi.org/10.1016/j.cemconcomp.2018.09.018>

Important note

To cite this publication, please use the final published version (if applicable). Please check the document version above.

Copyright

Other than for strictly personal use, it is not permitted to download, forward or distribute the text or part of it, without the consent of the author(s) and/or copyright holder(s), unless the work is under an open content license such as Creative Commons.

Takedown policy

Please contact us and provide details if you believe this document breaches copyrights. We will remove access to the work immediately and investigate your claim.

Green Open Access added to TU Delft Institutional Repository

'You share, we take care!' – Taverne project

<https://www.openaccess.nl/en/you-share-we-take-care>

Otherwise as indicated in the copyright section: the publisher is the copyright holder of this work and the author uses the Dutch legislation to make this work public.



Size effect on splitting strength of hardened cement paste: Experimental and numerical study

Hongzhi Zhang, Branko Šavija, Yading Xu*, Erik Schlangen

Microlab, Faculty of Civil Engineering and Geosciences, Delft, Netherlands

ARTICLE INFO

Keywords:

Micro-mechanical testing
Multiple length scales
Splitting tensile strength
Lattice modelling
Hardened cement paste

ABSTRACT

Cement paste possesses complex microstructural features including defects/pores over a range of length-scales, from nanometres to millimetres in size. As a consequence, it exhibits different behaviour under loading depending on the size. In this work, cubic specimens in a size range of 1: 400 were produced and tested by a one-sided splitting concept using different testing instruments. The smallest specimen with size of 100 μm showed a high nominal splitting strength (18.81 MPa), an order of magnitude higher than the measured strength of 40 mm specimen (1.8 MPa). The test results were used to fit existing analytical size effect models. Although a good fit can be found for the existing size effect models, special attention should be given to the physical meaning behind these empirical parameters. In addition, a multi-scale modelling strategy that considers microstructural features at different length scales was adopted to model the trend of decreasing strength with specimen size observed in experiments. A good agreement between experimental observations and modelling results indicates that the featured material structure dominates the observed size effect on measured strength in the size range considered.

1. Introduction

Cement paste is the basic binding material in concrete. Therefore, designing cementitious materials with proper performance depends to a large extent on good understanding of cement paste's behaviour. Although the fracture properties of cement paste have been studied extensively [1–4], a clear understanding of the deformation and fracture behaviour at different length scales is still lacking. This is because the overall material structure of cement paste covers multiple length-scales (ranging from sub-nanometres to metres) [5], and the fracture tests of laboratory sized samples (centimetre range in general) are not capable of investigating the influence of the material structure smaller than a few millimetres. Furthermore, it has been long known that strength and failure behaviour of quasi-brittle materials is size dependent [6]. The measured mechanical properties depend on the sample size and the featured material structures. Therefore, tests need to be performed at different length scales in order to understand the mechanical and fracture behaviour of such materials.

In practice, failure of cement paste is caused by the local tension [7]. It is therefore important to investigate the tensile strength at different length scales. For the centimetre sized samples, tensile strength is measured using a variety of test methods: uniaxial tension, Brazilian splitting, 3-point bending and 4-point bending. However, these

techniques are difficult to apply at the micro-scale, since the equipment is not suitable for manipulating components with sub-millimetre size [8]. Therefore, more suitable instruments and advanced test procedures need to be used.

Recently, use of a nanoindenter has been proposed by several researchers to measure the tensile strength of cement paste [9] and individual hydration phases [10] using micro-cantilever bending tests. This technique consists of specimen preparation using a focused Ga-ion beam milling. With this procedure, a micro-cantilever (with a triangular or rectangular cross-section depending on the procedure used) is created by milling the solid matrix. Typically, the size of these micro-cantilevers is up to 10 μm . The cantilevers are then subjected to bending by applying a load at the end of the cantilever using the nanoindenter. This provides a measure of the elastic modulus and the flexural strength of the micro-volume. Similarly, a micro-pillar compression technique involving focused ion milling of a micro-pillar in the material and a compression test using nanoindenter has been performed by Shahrin and Bobko [11] to measure the compressive strength and modulus of the C-S-H particles in the cement paste matrix. However, a major drawback of this approach is the time-consuming specimen preparation. Consequently, a relatively small number of specimens can be prepared and analysed [12]. Nevertheless, at small (i.e., micrometre) length scales, a high scatter of measured mechanical properties is

* Corresponding author.

E-mail address: Y.Xu-5@tudelft.nl (Y. Xu).

expected [13,14]. Therefore, a large number of tests need to be performed for the measurements to be statistically reliable.

The authors have recently developed a method that uses physical dicing to create a grid of micro-cubes (e.g. $100 \times 100 \times 100 \mu\text{m}$) on a glass substrate [14,15]. For estimating the splitting tensile strength of the micro-cubes, a one-sided splitting by a nanoindenter was performed [14]. In previous work, hundreds of micro-cubes were tested by applying the load across the middle axis on the top using a diamond cylindrical wedge tip. This technique provides an unprecedented opportunity for experimental investigation of fracture behaviour of this material with a significantly improved size range, as the most conventional size of cement paste specimen is around a few centimetres. In this work, hardened cement paste cubes of seven different sizes in a scale range of 1: 400 were produced and tested by this one-sided splitting concept with different test instruments.

During past decades, several analytical size effect models, such as Carpinteri's multifractal scaling law [16–18] and Bažant's size effect law [19–21], have been proposed to predict the strength decreasing with the structure size increasing. The first approach is based on considerations of the fractal geometry of the microcrack structure at peak stress [16], whereas the second method is established according to an energy balance relation [19]. Both models can give good estimations for the laboratory sized specimens and provide valuable input for the design of concrete structures. On the other hand, with the development of the advanced computer facilities and algorithms, numerical modelling has become a complementary approach to investigate the size effect. The use of an experimentally informed discrete model which takes the material structure into account provides an insight into the relation between material structures and fracture process [22,23]. With recent advantages in parallel computing, a 3D lattice fracture model has been used for studying size effect in concrete [24,25]. Although the approach is promising, the size range analysed so far is relatively small (1:8) due to (still) huge computational demands. In order to broaden the size range in which such discrete model can be used, a multi-scale modelling strategy developed by the authors [26,27] has been adopted herein to simulate the fracture performance of specimens over two length scales. Microstructures at different length scales were captured by X-ray computed tomography (XCT) and used as input in the model. The modelling results were compared with those obtained experimentally, showing a good agreement. With the large size range of fracture testing and multi-scale modelling of cement paste cube under one-sided splitting, the existing analytical size effect models can be examined and a new insight into the influence of featured material structures at different length scale on the fracture performance is provided.

2. Experimental

2.1. Materials and sample preparation

The tested material was a 28-day-old standard grade OPC CEM I 42.5 N paste with 0.4 water-to-cement ratio. Cubic specimens of different sizes (0.1 mm, 0.2 mm, 0.5 mm, 5 mm, 10 mm, 20 mm and 40 mm, see Fig. 1) were prepared for the one-sided splitting test. Cement and deionized water were mixed for 1 min at low speed and 2 min at high speed. The fresh mixtures were poured into two types of PVC cylinders: a cylinder with a diameter of 60 mm and a height of 120 mm was used to fabricate specimens larger than 20 mm, while smaller specimens were obtained from a cylinder with diameter of 24 mm and height of 39 mm. In order to minimize bleeding, the samples were rotated at a speed of 2.5 revolutions per minute for 24 h. Afterwards, the cement paste cylinders were stored for curing in sealed conditions at a temperature of $22 \pm 2 \text{ }^\circ\text{C}$. After 28 days, they were demoulded and cut using a diamond saw into final cubic size at meso-scale (5 mm, 10 mm, 20 mm and 40 mm) as shown in Fig. 1a, while a more complicated fabrication process was used for the preparation of micro-scale cubic specimens (0.1 mm, 0.2 mm, 0.5 mm). The readers are referred to Ref.

[15] for a detailed description of the fabrication process. In short, the specimens were prepared in two steps. First, cement paste slices with a thickness of 2 mm were cut from the cylinder and bound to a glass substrate. This was followed by repeated grinding and polishing until a thickness equal to the height of the desired cubic specimens and a flat surface were reached. Finally, a micro-dicing saw was used to cut through the slice from two perpendicular directions to generate an array of micro-cubes on the glass substrate. The distance between two parallel cuts was chosen as the sum of the blade thickness ($260 \mu\text{m}$) and the length of the desired cubic specimens. Environmental scanning electron microscope (ESEM) images of the $200 \mu\text{m}$ and $100 \mu\text{m}$ cube array are shown in Fig. 1b and c. The images were taken in back-scattered electron (BSE) mode using 20 kV accelerating voltage with 10 mm working distance and the magnification was $100 \times$.

2.2. One-sided splitting test

The setup of the one-sided splitting test is similar to the Brazilian test (NEN-EN 12390-6 Standard) for splitting tensile strength assessment of cementitious materials. As shown in Fig. 2, the difference is in the boundary condition at the bottom: in the standard Brazilian test, a linear support is used; for the micro-cube splitting test, the specimen is clamped (glued) to the bottom. In order to undertake this set of mechanical tests across several length-scales, three arrangements were used herein.

The first is an Agilent G200 Nanoindenter. A diamond cylindrical wedge tip (radius $9.6 \mu\text{m}$) was used to apply the load across the middle axis of the micrometre sized specimens glued on the glass. A tip with a length of $200 \mu\text{m}$ was adopted for testing the cubes of $100 \mu\text{m}$ and $200 \mu\text{m}$, while cubes of $500 \mu\text{m}$ were split by a wedge tip with a radius of $50 \mu\text{m}$ and a length of $700 \mu\text{m}$. The experiments were run using displacement control with a loading rate of 50 nm/s . Fig. 3a presents the fractured specimens observed by the ESEM. Since large scatter is expected for the micrometre sized specimens, 100, 60 and 30 specimens were fabricated and tested for $100 \mu\text{m}$, $200 \mu\text{m}$ and $500 \mu\text{m}$ cubes, respectively. A typical load-displacement curve of the smallest sample is presented in Fig. 3b. The curve shows two distinct regimes. In regime I, a nearly linear load-displacement curve is observed until the peak. This is followed by an unstable regime (regime 2), which signifies a rapid crack propagation and failure of the micro-cube. This unstable failure could be caused by the following: 1) the displacement control is not fast enough to measure a post-peak behaviour; 2) the behaviour of the sample might be brittle, but the system cannot capture a snap-back.

Meso-scale cubic specimens with 5 mm and 10 mm length were tested by the second instrument, a mini tension/compression stage. Two-component glue X60 consisting of a power Plex 7742 and a fluid Pleximon 801 was used to glue the sample on the test stage. A steel bar (radius: 0.5 mm) was placed between the loading stage and the specimen to impose a line load on one end. The test was performed under deformation control with a constant loading rate of 0.01 mm/s 15 and 10 specimens were tested using this set up for the 5 mm and 10 mm cube size, respectively. Fig. 3c and d show a cracked 10 mm cubic specimen on the stage and its load-displacement curve. The failure mode is the cube split into two halves and a relatively brittle post-peak behaviour is observed.

For testing of larger specimens (20 mm and 40 mm), an Instron 8872 loading device was used. For the sake of consistency of applied boundary conditions, the specimens were glued to the bottom steel plane using the same adhesive used in the 10 mm cubic specimen test, while a steel bar with a 2 mm radius was applied at the top (see Fig. 3e). A constant loading speed of 0.03 mm/s was used and 10 specimens for each size family were tested. In Fig. 3f, a typical load-displacement curve is presented in which a similar brittle post-peak as specimens tested by the mini tension/compression stage is found.

A consistent crack pattern is observed for all tested specimens. Although a brittle post peak behaviour is measured for specimens larger

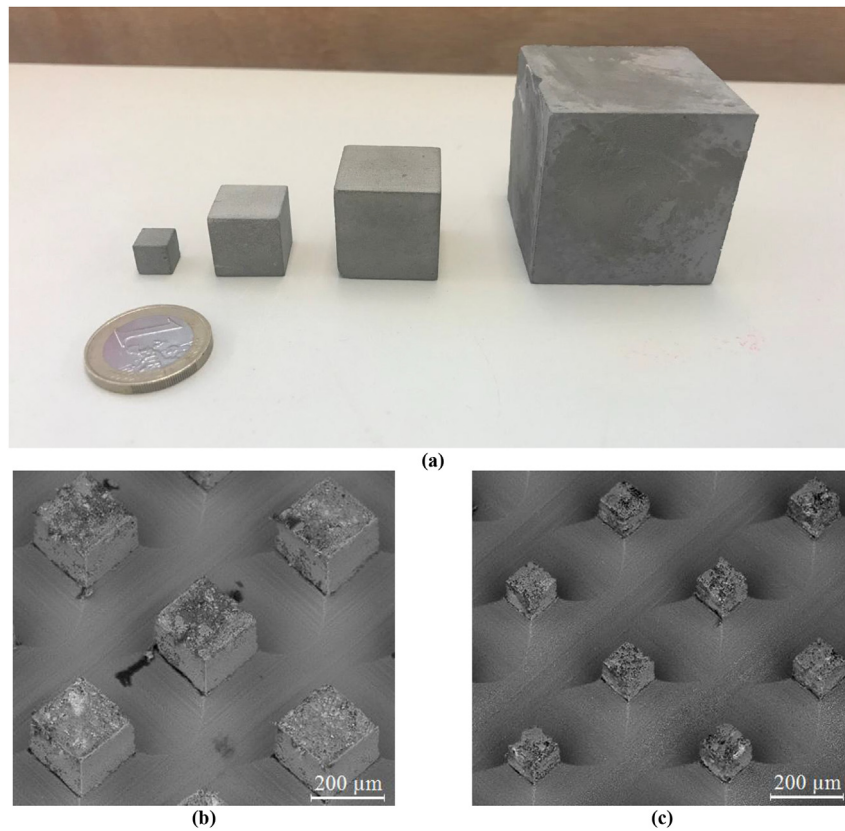


Fig. 1. Specimens with size range of 1: 400 (a) cubic specimens with size of 5, 10, 20, 40 mm; (b) ESEM image of sample size of 200 μm (c) ESEM image of specimens with size of 100 μm.

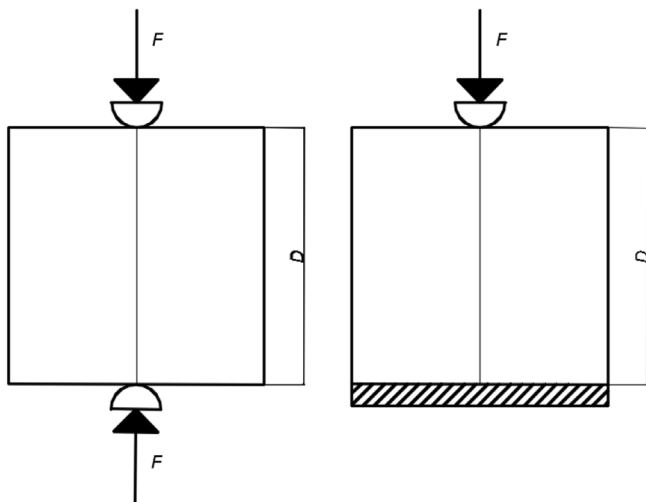


Fig. 2. Schematics of the Brazilian splitting test (left) and the one-sided splitting test (right), after [28].

than 5 mm, no post peak behaviour could be measured by the nanoindenter for smaller specimens. Furthermore, it should be noticed that the displacement was measured directly from the machine. This means that the measured displacements could be affected to a certain extent by the stiffness of the loading frame, which cannot be eliminated. Thus, in this work the focus was only on the splitting strength which was calculated from the peak load P . As previously shown by the authors [14], the strength estimation of such test can be analogous to the Brazilian splitting test:

$$f_{st} = \frac{2P}{\pi D^2}, \tag{1}$$

where D is the dimension of the cube. As the bottom side is glued in this case, a somewhat different stress distribution occurs, leading to a modified equation:

$$f_{st} = \alpha \frac{2P}{\pi D^2}. \tag{2}$$

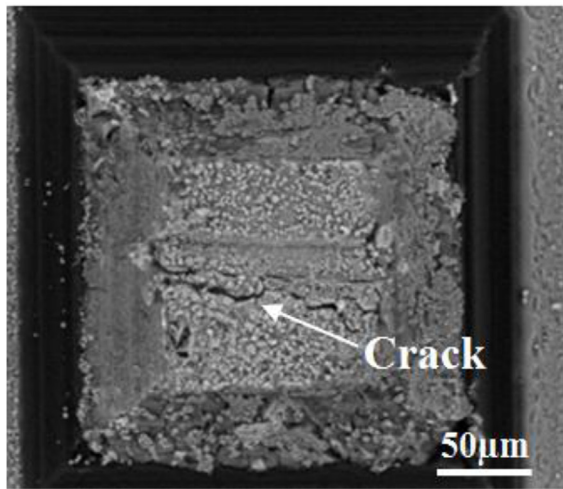
where α is estimated as 0.73 from a finite element model, assuming a linear elastic, homogeneous, and isotropic material. Note that this parameter was used for strength estimation for all specimens over the examined size range, although the cement paste specimens can hardly be considered as homogeneous at any of the size examined. The influence of heterogeneity on the mechanical behaviour at different length scale is discussed later. Therefore, Equation (2) was used to estimate the splitting tensile strength of all specimens along the tested range.

2.3. Material structure characterization

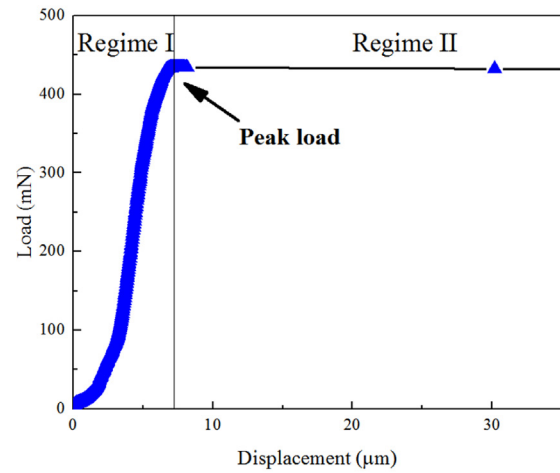
The mechanical properties of cement paste are affected by various factors at different length scales. In order to understand better the influence of material structure on the decrease of strength with specimen size, the material structure informed lattice fracture simulation was performed as described in Section 3.1. As input, material structures of cement paste at two levels of observation, i.e., micro- and meso-scale, were captured by X-ray computed tomography (XCT) scanning of different sized specimens. Consequentially, different voxel sizes of material structure as well as material structures were obtained.

2.3.1. Micro-scale material structure

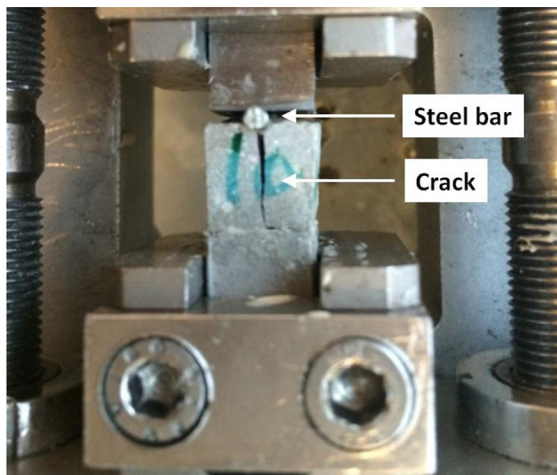
At the micro-scale, multiple hydration products and capillary pores can be observed in the cement paste matrix. Therefore, a multi-phase



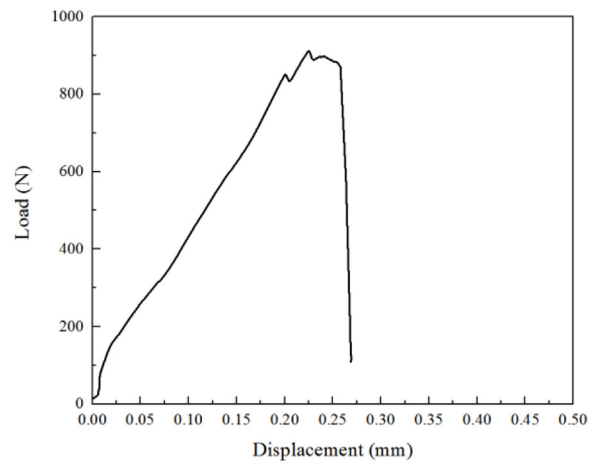
(a)



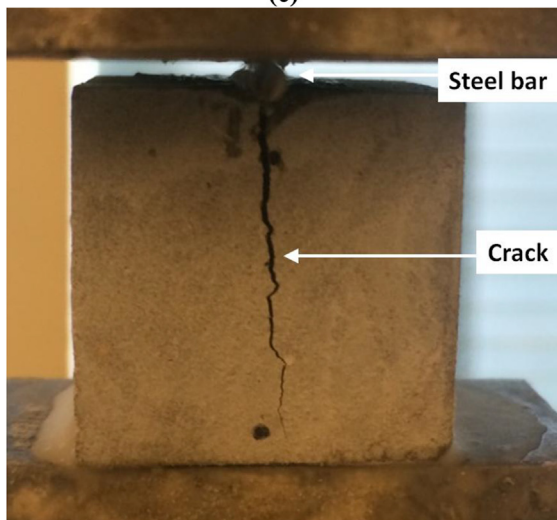
(b)



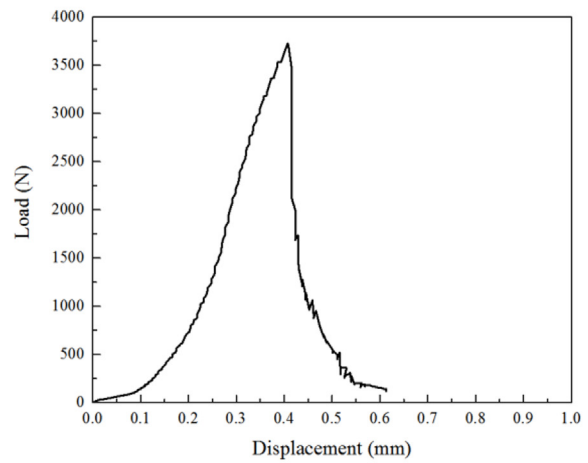
(c)



(d)



(e)



(f)

Fig. 3. Test configurations for the one-sided splitting test: (a) a cracked 100 μm cement paste cube observed by ESEM; (b) a typical load - displacement curve measured by nanoindenter [28]; (c) a cracked 10 mm cube on the mini tension/compression stage; (d) a typical load - displacement curve measured by the mini tension/compression stage (e) a cracked 40 mm specimen on the loading device; (f) a typical load - displacement curve measured by the Instron loading device.

microstructure should be considered at this scale. Herein, digital material structure consisting of anhydrous cement grains, inner and outer hydration products and capillary pores was captured by scanning a prism with a cubic cross-section size of 500 μm using XCT. As the focus

of current work is on utilization of the digital material structure as input for the discrete fracture model to simulate the size effect on material strength, the readers are referred to [15] for the detailed description of the XCT experiment and segmentation of cement phases. In order to

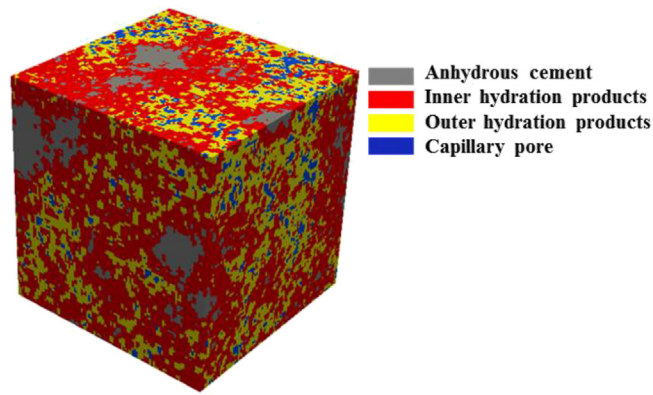


Fig. 4. An example of a segmented hydrated cement paste microstructure of specimen with the size of $100\ \mu\text{m} \times 100\ \mu\text{m} \times 100\ \mu\text{m}$ extracted from XCT [15].

Table 1
vol fractions of segmented microstructures.

Porosity	Anhydrous cement	Inner hydration products	Outer hydration products
0.1184	0.1064	0.4530	0.3222

validate the fracture simulation using experimental data, cubic volume with size of $100\ \mu\text{m}$ ($50 \times 50 \times 50$ voxels) was extracted to match the size of smallest specimen which can be produced and measured experimentally (see Fig. 4). A resolution of $2\ \mu\text{m}/\text{voxel}$ was chosen to optimize the computational demands of the lattice fracture simulation. Although this resolution is not as high as others reported [29,30], it is sufficient to model the fracture behaviour of hardened cement paste at micro-scale and consider its heterogeneity [31]. The segmented amount of each phase (by volume) for the scanned prism is listed in Table 1 and the hydration degree is estimated as 0.75 [15]. In order to consider the stochastic nature of this material, 10 digital cubic specimens were extracted and tested by the fracture model. These digital cubic specimens were then used as input in the lattice model. Note that, for each cubic specimen, different relative amount of each phase is present as a result of the heterogeneous nature of cement paste.

2.3.2. Meso-scale material structure

For the material structure at meso-scale, a cylindrical specimen with a diameter of 24 mm was scanned with a resolution of $100\ \mu\text{m}/\text{voxel}$ using XCT. Voltage of 130 Kev and current of $150\ \mu\text{A}$ for the X-ray source tube was used during the scanning. After image reconstruction, a binary microstructure comprising air (i.e. entrapped air void or large capillary pore) and homogenised cement paste matrix was segmented from the initial greyscale images. The first inflection point in the cumulative fraction curve of greyscale level was used for the thresholding [29,32]. In this way, total porosity of 5.29% (large pores only) was obtained for the scanned specimen. 5 mm cubic volume (i.e., $50 \times 50 \times 50$ voxels) was randomly extracted from the scanned volume to be used as input in the fracture simulation (see Fig. 5). Note that the resolution at the meso-scale was chosen to match the size of the investigated size of material volume at the micro-scale. In such a way, a multi-scale fracture modelling approach developed and validated by the authors can be implemented. The number of voxels was kept constant for the digital cubic specimens in different scales to explicitly show the influence of featured material on the predicted mechanical response. 10 cubic volumes were randomly extracted for fracture simulation to investigate the fluctuation of simulated results.

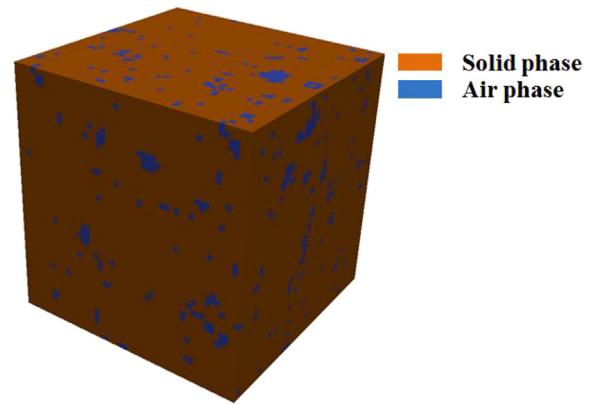


Fig. 5. Material structure of specimen with size of $5\ \text{mm} \times 5\ \text{mm} \times 5\ \text{mm}$ extracted from XCT experiment.

3. Modelling

In general, size effect is related to the number and nature of crack initiation sites (the statistical size effect) sampled by a given size test specimen as well as the size and spacing of the formed strain localization zones (the energetic size effect). With respect to a homogeneous microstructure, the measured strength is associated with local defects and cracks before the peak load. However, cement-based materials are a more extreme case because as specimen size increases, different features of the bulk material are sampled so that the measured ultimate properties will be influenced by different microstructural features. For example, in the micro-scale specimens, the capillary pores (up to a few hundred micrometres) play a primary role in the fracture process, while in the meso-scale specimens, the big pores (larger than a few hundred micromeres) dominate the measured mechanical properties, especially the strength. To model the deformation and fracture of cement paste, it is necessary to capture the microstructure of such material at multiple length-scales, which is currently not possible using a single length-scale approach. Therefore, a multi-scale modelling strategy considering different featured complex microstructure of cement paste proposed by the authors [13,33] was adopted herein.

3.1. Model description

By means of methods derived from statistical physics, lattice-type models are generally used to address the role of disorder in quasi-brittle materials [34]. It is found that this type of fracture model is quite useful in investigation of size effect on the fracture mechanism because of its inherent simplicities [22–24]. These simplicities include the purely elastic-brittle fracture behaviour assumption of local lattice elements and a straightforward implementation of the material heterogeneity at various levels of observation. This allows to study fracture mechanisms and the size effect on fracture in the same way as in the laboratory [24].

In the current version of Delft lattice fracture model, the material is schematized with a network of Timoshenko beams which take the shear deformation into account [27]. The network is generated as follows. First, the nodes are positioned randomly inside the cells of a grid with regular cell size. Then, Delaunay tessellation of the domain is performed in order to generate the lattice mesh [35]. A randomness number defined by the ratio between size of the sub-cell and the main cell is generally introduced to describe the degree of disorder of lattice mesh. With respect to a regular lattice, the randomness equals zero and the nodes are positioned in the centre of the main cell resulting in a lattice mesh wherein no disorder is present. For an irregular lattice mesh, all elements of the mesh have different lengths and, thus, different stiffness, disorder is already introduced at the ‘geometrical’ level [36]. Material heterogeneity is introduced using a particle overlay

procedure [37]. In this study, a material structure generated by XCT was used. This procedure defines the type of each lattice element according to the values of two voxels corresponding to its end nodes, which is further used to define properties of each lattice element. A particular external boundary displacement can be applied, and a set of linear elastic analyses is performed by calculating the stress within each lattice element as:

$$\sigma = \alpha_N \frac{N}{A} + \alpha_M \frac{\max(M_x, M_y)}{W}, \tag{3}$$

where *A* denotes the beam cross-sectional area, *W* is the section modulus; *N* is the normal force along the element. *M_x* and *M_y* are the maximum internal bending moments. α_N and α_M represent the normal force influence factor and the bending influence factor. Their values are commonly adopted as 1.0 and 0.05, respectively. These values were also adopted herein. The influence of different values of these parameters on the concrete fracture response is discussed elsewhere [38]. In every analysis step, loading is increased until exactly one beam in the mesh has a stress/strength ratio equal to one. This beam is then removed from the mesh. The mesh is then updated and relaxed. This loading procedure is repeated until a pre-defined stopping criterion (in terms of, e.g., load or displacement) is met. Consequently, the fracture pattern of the investigated material volume at each step can be obtained as well as their load-displacement response.

3.2. Multi-scale modelling approach

With recent advantages in multi-scale modelling [13,33], material structures at different levels of observation can be implemented. By properly choosing a volume size of material structure at small scale which matches the smallest feature of the larger scale observation, the global fracture behaviour (i.e., load-displacement response under uniaxial tension) of smaller scale simulation can be used as input local mechanical properties for the fracture modelling at larger scale (see Fig. 6). It is worth emphasizing that this methodology does not consider the representative volume element (RVE) of cement paste. This is because, for fracture of softening materials, an RVE might not exist due to localization issues [39]. The simulation strategy using two scale digital material structures is as follows:

Firstly, a lattice mesh with randomness of 0.5 was generated on the basis of a 50 × 50 × 50 cubic grid. This mesh was used for fracture simulation of all specimens at both micro-scale and meso-scale to investigate the influence of material structure on the fracture behaviour (i.e., without considering possible effects of mesh randomness which could occur if different mesh realizations were used).

Afterwards, the material structures generated in Section 2.3 were

Table 2

Assigned local mechanical properties of individual phases at micro-scale [15].

Phase	Young's modulus (GPa)	Tensile strength (MPa)
Anhydrous cement	99	683
Inner hydration product	31	92
Outer hydration product	25	58

overlaid on the mesh for assigning mechanical properties of each local element accordingly. Pores or air voids were considered as initial flaws in the material. Consequently, an element with an end node in a void/pore phase voxel was removed from the mesh. As the beam element was assumed to be perfectly brittle in the simulation, only tensile strength and elastic modulus of discrete phases were needed as input.

For the micro-scale simulation, six types of lattice elements were determined by the three phases. Elastic modulus of a beam element was estimated as a harmonic average of the connected two phases, while the lower value of the two phases was considered as tensile strength [40,41]. Table 2 lists the mechanical parameters of each single phase. Elastic moduli were taken from nanoindentation measurements for individual phases as reported by Hu et al. [42]. The tensile strengths of lattice elements were calibrated in the authors' previous work [15], wherein experimental measurements were used as a basis for inverse analysis. These values were validated by the authors in both micro-mechanical and multi-scale modelling [14,33]. Similar values are reported by Hlobil et al. [43] for a multi-scale fracture modelling of blended cement paste. With these assumptions, six types of elements are generated as listed in Table 3.

For the mesoscale fracture simulation, 10 types of lattice elements were randomly distributed in the lattice network (after removing element corresponding to the air phase). Their mechanical properties, i.e., elastic modulus and tensile strength (see Table 4), were taken from the computational uniaxial tension test of the corresponding micro-scale specimens which have been reported in Ref. [31]. For simplification, the average of modelling results from three directions was used to represent the specimen's micromechanical properties. In order to focus on the influence of the microstructural features on the fracture behaviour, the constitutive law of local element was assumed to be linear elastic-perfectly brittle.

The one-sided splitting boundary conditions was assigned to the specimens at both length-scales, as shown in Fig. 7. The nodes at bottom surface were clamped to represent the glued sample on the plate and a prescribed vertical displacement was applied on nodes in the two lines closed to the middle axis of the top surface to mimic the indenter load. The glue between the specimens and glass substrate was not considered in this work, as it is found by the authors that its influence on the predicted strength is negligible, although it does influence the deformation of the loading point significantly [14].

4. Results and discussion

4.1. Experimental results and discussion

Table 5 presents the measured average strength of each size family together with their standard deviation and coefficient of variation (CoV). As a result of the small volume of material sampled, a large scatter in measured strength is found for the specimens at small scale. Clearly, the average strength of the micro cube (100 μm) is one order of magnitude larger than the strength of the laboratory (i.e. centimetre sized) sample. Since the size of specimens is below a few hundred micrometres, they are free from large capillary pores and air voids which significantly reduce the mechanical performance of the material [33]. With increasing specimen size, the standard deviation and CoV decrease, as well as the measured strength. As the failure of micro-scale sized samples largely depends on the spatial distribution of micro-scale

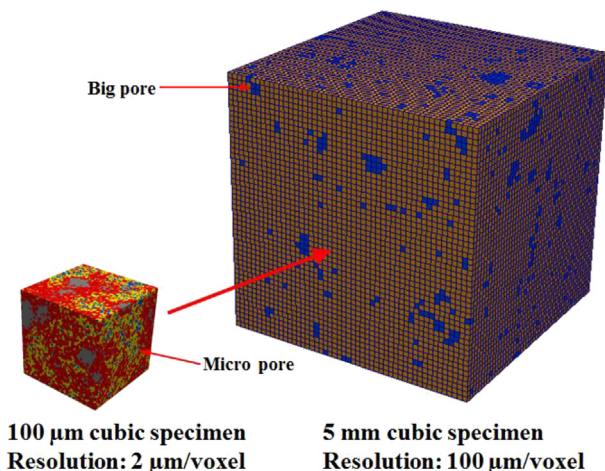


Fig. 6. Schematic illustration of the multi-scale modelling strategy.

Table 3
Lattice element types and their mechanical properties [15].

Element type	Phase 1	Phase 2	Young's modulus (GPa)	Tensile strength (MPa)
A-A	Anhydrous cement	Anhydrous cement	99	683
I-I	Inner hydration product	Inner hydration product	31	92
O-O	Outer hydration product	Outer hydration product	25	58
A-I	Anhydrous cement	Inner hydration product	47	92
I-O	Inner hydration product	Outer hydration product	28	58
A-O	Anhydrous cement	Outer hydration product	40	58

Table 4
Element types used for the fracture simulation of 5 mm specimens (obtained in Ref. [31]).

Element type	Young's modulus (GPa)	Tensile strength (MPa)
1	21.47	21.13
2	19.20	16.72
3	23.13	18.85
4	22.20	20.81
5	19.01	15.19
6	21.03	19.45
7	24.24	20.12
8	20.04	17.40
9	22.26	22.03
10	18.10	14.63

pores, a large scatter in measured data is present. In the meso-scale specimens, a relatively large population of micro-scale pores exists, therefore their distribution has less impact on the strength and potentially allows more micro-cracks to occur and coalesce before final fracture [44].

Because of the high scatter that exists in the small size (≤ 0.5 mm) specimens, it is advised to present the strength at the small scale by its probability distribution rather than the average value [14]. Herein, a two-parameter Weibull analysis was performed as the fracture is mostly governed by the weakest spot, i.e., pores, which can be written as [45]:

$$P_f = 1 - \exp \left[- \left(\frac{\sigma_f}{\sigma_0} \right)^m \right] \quad (4)$$

where P_f is the probability of failure, m the Weibull modulus (shape parameter) used to describe variability in measured material strength, σ_f the fracture strength and σ_0 is the scaling parameter (characteristic strength). As reported in Refs. [46,47], in the absence of specific requirements, approximately 30 test specimens can provide adequate Weibull distribution parameters and more specimens contribute little towards better uncertainty estimates. Considering the number of specimens tested in each size group (0.1 mm, 0.2 mm and 0.5 mm), a good regression can be expected if the strength of cement paste at micro-scale can be represented by the two-parameter Weibull statistics. The estimated regression parameters are listed in Table 6 with a high determination coefficient. This indicates that only one type of flaw exists in the material at this scale - the micro-pore [46]. A similar Weibull modulus is found for the three specimen sizes considered. The small difference among the three size families could be caused by the heterogeneity of the solid phases and the interaction between cracks, or between cracks and the gradient of the stress field [48]. The fracture probability of three size specimens are compared in Fig. 8. It is apparent that, on one hand, regarding the same fracture strength (below 30 MPa), the smaller specimen has a lower fracture probability. On the other hand, for the same fracture probability, the smaller specimen tends to yield a higher strength.

4.2. Fitting of analytical size effect models

The large size range (1: 400) of experimental data allows an examination of existing size effect models for brittle and quasi-brittle

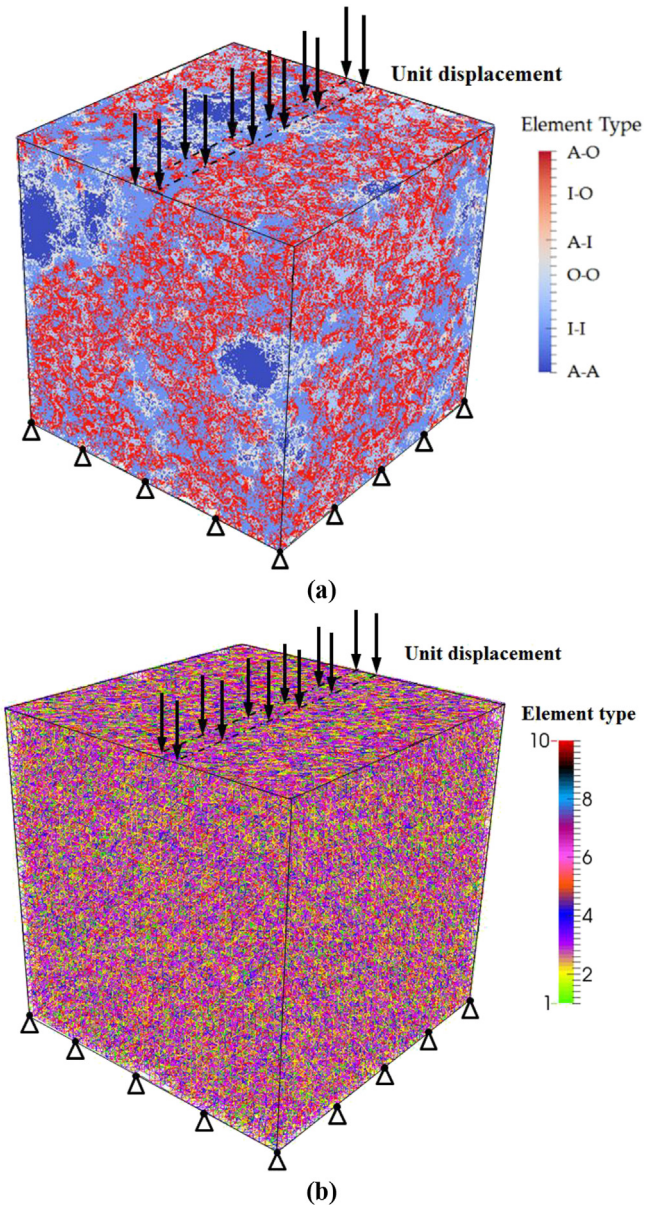


Fig. 7. Boundary conditions of one-sided splitting test on two scale specimens: (a) micro-scale specimen; (b) meso-scale specimen.

materials, which need to be fitted by experimental data. Among them, the most popular approaches are the Weibull statistical theory [49], multifractal scaling law (MFSL) developed by Carpinteri [16–18] and Bažant's size effect law [19].

4.2.1. Weibull size effect

The most well-known theory considering the statistical size effect caused by randomness of material strength is the Weibull statistical

Table 5
Summary of test results of each specimen size.

Cubic size (mm)	Number of tested cubes	Average strength (MPa)	Standard deviation	CoV
0.1	100	18.81	3.95	0.210
0.2	60	14.84	2.71	0.182
0.5	30	10.75	1.89	0.176
5.0	15	4.92	0.82	0.170
10.0	10	3.90	0.61	0.156
20.0	10	1.80	0.26	0.144
40.0	10	1.18	0.16	0.135

Table 6
Fitting results of the distribution of small size sample.

Family size (mm)	m	σ_0	R^2
0.1	5.376	20.27	0.9966
0.2	6.103	15.60	0.9920
0.5	6.089	11.54	0.9912

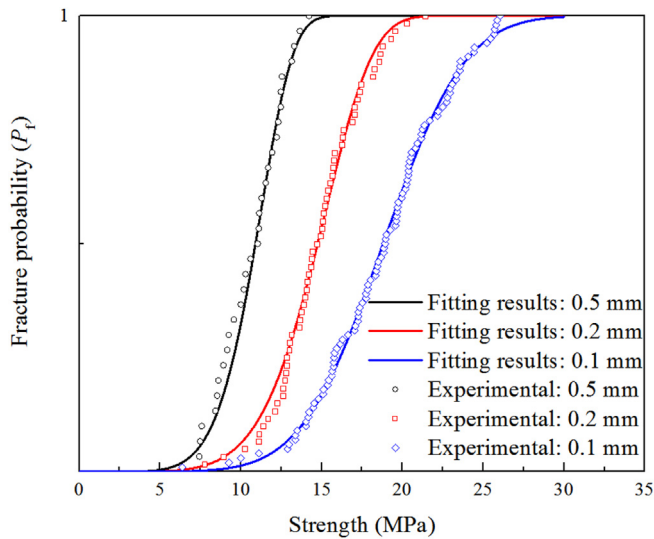


Fig. 8. Fracture probability of cubic specimens with size of 0.1 mm, 0.2 mm and 0.5 mm.

theory [49], also known as the weakest link theory. This theory assumes that the entire structure will fail once the first (i.e., the weakest) element fails. On the basis of statistics, the nominal strength σ_N shows the following relationship with the structure size D [50]:

$$\sigma_N(D) \propto D^{-\frac{n}{m}} \tag{5}$$

where m is the Weibull modulus which can be found by a fit on experimental data and n denotes the number of dimensions. In case of three-dimensional similarity like in the present investigation, $n = 3$. When the nominal strength and the size are presented in a bi-logarithmic plot, the parameters can be approximated with a linear expression:

$$\log \sigma_N = a - \frac{n}{m} \log D. \tag{6}$$

In the current work, the linear regression was performed using a Trust-Region method [51]. As shown in Fig. 9, the best fit shows a high determination coefficient $R^2 = 0.9886$ and gives an estimation of the Weibull modulus $m = 8.1$. Note that if the measurements show little variation from sample to sample, the calculated Weibull modulus will be high and a single strength value would serve as a good description of the sample-to-sample performance. Apparently, this is not the case for

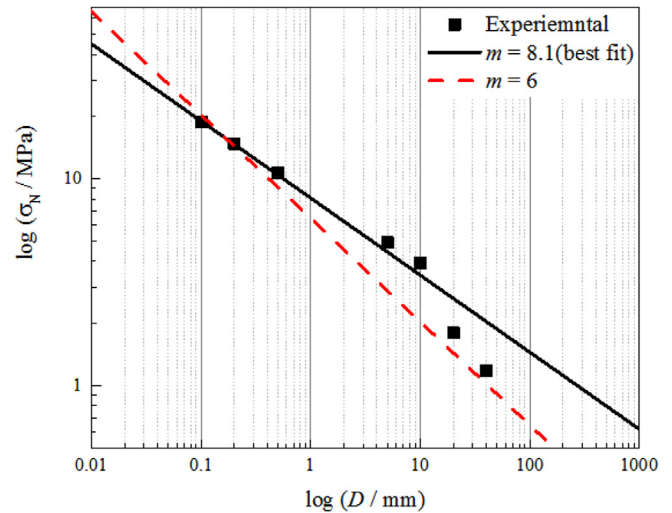


Fig. 9. Fit of Weibull weakest link theory.

cement paste. Without presence of stiff aggregate which enables a more stable crack propagation, cement paste is weaker and shows higher scatter, thus its Weibull modulus is lower than that of concrete (i.e., 12 as reported by Zech and Wittmann [52]). It has been shown by Van Vliet et al. [53] that a Weibull size effect is applicable for concrete in uniaxial tension. In their work, $m = 12$ and $n = 2$ were directly used to fit the Weibull size effect theory and showed good agreement with experimental data. Herein, a Weibull modulus $m = 6.0$ was estimated from Section 4.1 for the cement paste, which makes the slope value -0.5 in the $\log \sigma_N$ - $\log D$ plot as $n = 3$. A determination coefficient of 0.9536 is found meaning a good linear regression exists in the analytical equation and the measured nominal splitting strength. As m is assumed from the micro-scale specimens, a better agreement is found at this size range, while a relatively large discrepancy is observed at the meso-scale. This is because the complex microstructural features of specimens change with the specimen's size increasing.

4.2.2. Carpinteri's multifractal scaling law

Based on considerations of the fractal structure of material and its effect on mechanical behaviour, Carpinteri and his co-workers developed the multifractal scaling law (MFSL) [34–36]. According to MFSL, the nominal strength σ_N under tension decreases with increasing the characteristic structure size D , which can be expressed as the following equation:

$$\sigma_N(D) = f_t \sqrt{1 + \frac{l_c}{D}} \tag{7}$$

where f_t and l_c are empirical constants to be determined from tests. f_t presents the tensile strength of the structure with infinitely large size and l_c denotes a characteristic length representing the influence of disorder on the mechanical behaviour. When D is below the characteristic length scale l_c , a strong size-scale effect is provided by the influence of disorder which results in a slope of -0.5 on a $\log \sigma_N$ - $\log D$ diagram. Whereas, when D is higher than l_c , the size effect vanishes, and the MFSL grows toward a horizontal asymptote where a constant value of the strength is attained. As shown in the $\log \sigma_N$ - $\log D$ plot (Fig. 10), Equation (7) is fitted by the Trust-Region method. The best fitted curve with a determination coefficient (R^2) of 0.9676 predicts $f_t = 2.385$ MPa and $l_c = 6.823$ mm (Table 8). Although the determination coefficient is high, the tensile strength of the material for larger specimens is higher than the experimentally measured results of the largest specimens ($D = 40$ mm) herein. For a more reasonable fitting, the following two cases are assumed for f_t : 1) as same as the measured results of the largest specimens (1.2 MPa); 2) 70% of the measured

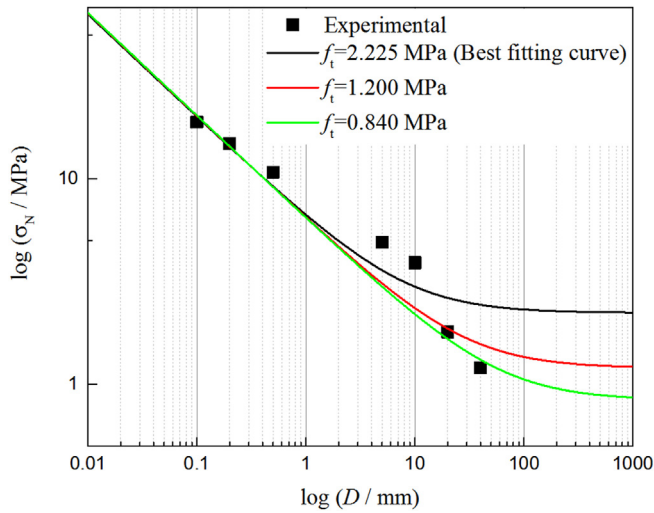


Fig. 10. Fits of Carpinteri's MFSL with different f_t .

Table 7

Fitting results of Weibull size effect.

Case number	m	a	R^2
1	8.10	8.05	0.9886
2	6.00	6.44	0.9536

Table 8

Fitting results of MFSL.

Case number	f_t (MPa)	l_c (mm)	R^2
1	2.225	8.017	0.9676
2	1.200	28.36	0.9616
3	0.840	58.30	0.9530

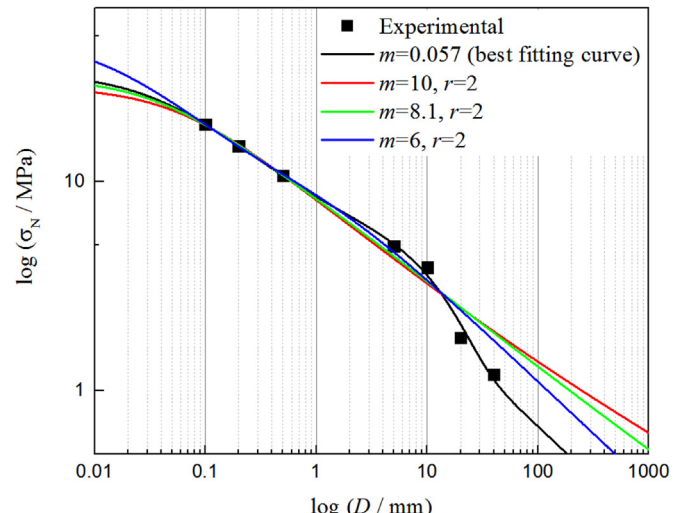
strength of the largest specimens (0.84 MPa) for linear regression respectively. Note that the value of 70% strength of largest specimen is only an estimation to show the influence of f_t on the curve fitting process, as the parameter f_t cannot be measured neither estimated accordingly. A determination coefficient higher than 0.95 is observed for both regressions, while a big difference in l_c is found with decreasing f_t . Thus, a reasonable estimation of f_t is necessary for a proper fitting of such model.

4.2.3. Bažant's energetic-statistical size effect theory

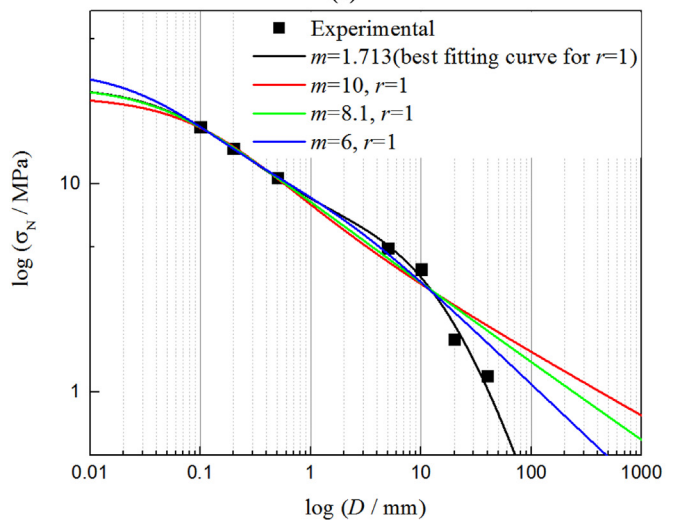
According to Bažant and his co-workers [20,21,54], there are two (independent) sources of size effect in brittle and quasi-brittle materials: energetic and statistical. The energetic (also known as deterministic) size effect is caused by formation of a region of intense strain localization with a certain volume, i.e., fracture process zone (FPZ). In turn, the statistical size effect is a result of the randomness of material strength as described above, which can be expressed by the Weibull weakest link theory. Combining the size effect and Weibull statistical theory, a general energetic-statistical size effect theory (ESSET) [20] can be written as:

$$\sigma_N(D) = f_r \left(\left(\frac{L_0}{D + L_0} \right)^{\frac{r \times n}{m}} + \frac{r D_b}{D + l_p} \right)^{\frac{1}{r}}, \tag{8}$$

where f_r , L_0 , l_p , D_b and r are empirical constants to be determined from tests. f_r is the nominal strength for very large structures (assuming no Weibull statistical size effects). L_0 is the statistical characteristic length, controlling the transition from constant properties to local Weibull statistic via strength random field, while D_b drives it from elastic-brittle



(a)



(b)

Fig. 11. Fits of Bažant's ESSET with different m : (a) $r = 2$; (b) $r = 1$.

to quasi-brittle. l_p represents the characteristic length of the micro-structure influencing both the size and spacing of localized zones, which is introduced to satisfy the asymptotic requirement to have a finite plastic limit when D approaches infinite size. Exponent r is a geometry-dependent factor, which controls both the curvature and the slope of the size effect and is constant when geometrically similar structures are considered.

This analytical equation is regarded as the asymptotic matching of large-size statistical and small-size deterministic size effects as it satisfies the following three asymptotic conditions: (1) for small sizes $D \rightarrow 0$, the asymptotic prediction reaches the plastic limit; (2) for large sizes $D \rightarrow \infty$, the Weibull size effect become dominant; (3) for $m \rightarrow \infty$ and $L_0 \rightarrow \infty$, the prediction leads to a deterministic size effect law. Fig. 11 presents the best fit of equation using Equation (8). Although a high determination coefficient (0.9992) is found, the Weibull modulus m is below 0.1, which is obviously unrealistic. Furthermore, although it is reported that the value of r should be close to 1 for two dimensional beams [20,55], the value for the cubic specimen is unknown. Thus, several assumptions on m were made with $r = 2$ (from the best fit curve in the current work) and $r = 1$, respectively. The fitted results were listed in Table 9. The value of m controls the slope at the large size range and a higher value of m corresponds to a gentler decrease of strength with the size increasing which means a more disordered

Table 9
Fitting results of the empirical parameters in Equation 8.

Case number	f_r (MPa)	L_0 (mm)	m	D_b (mm)	l_p (mm)	r	R^2
1	5.73	759.5	0.0566	0.6947	0.04214	2	0.9992
2	5.05	0.7549	10	1.083	0.06969	2	0.9934
3	6.92	0.741	8.1	0.4755	0.048	2	0.9944
4	9.02	1.133	6	0.1954	0.01371	2	0.9962
5	6.822	19.61	1.713	0.3744	0.1122	1	0.9991
6	7.097	0.6107	10	0.4386	0.1617	1	0.9915
7	9.45	0.557	8.1	0.2045	0.09583	1	0.9936
8	9.635	1.269	6	0.1558	0.05734	1	0.9963

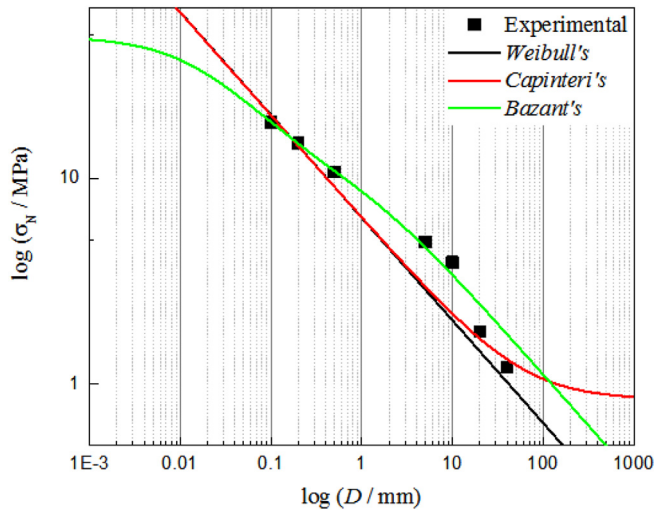
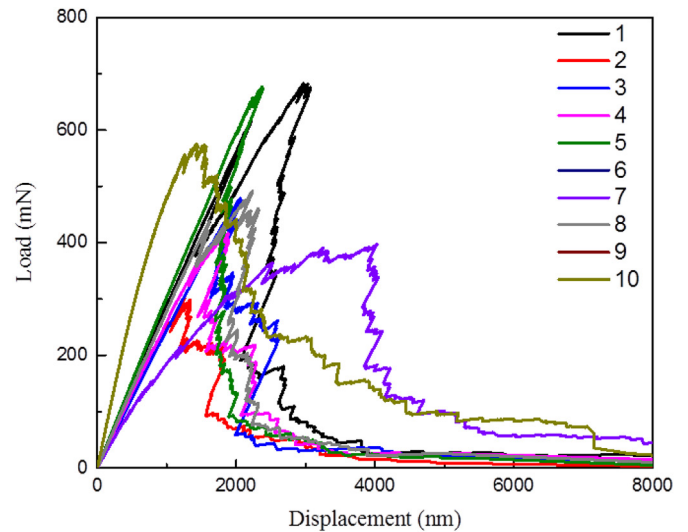


Fig. 12. Comparison of the fitting result of three analytical models.

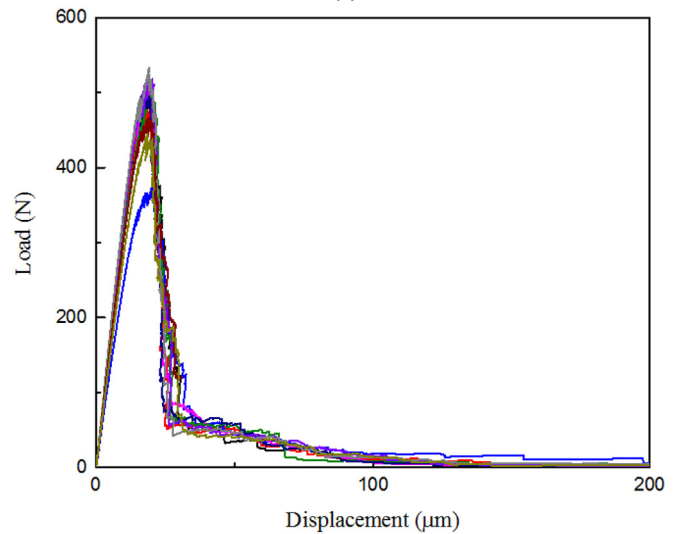
material has a stronger size effect on the strength decreasing. For the same m value, the cases in which $r = 1$ predicts a higher f_r . Note that the predicted f_r in Table 9 is higher than the f_c (2.225 MPa) predicted in Section 4.2.2 by the MFSL, because the nominal strength for very large structures in the Bazant's ESSET does not take the statistical size effects into account. Although, it is suggested that f_r should be calculated from the finite element modelling [20], this cannot be achieved with current test technique. As the influence of the randomness of strength distribution within the material cannot be eliminated from the experimental measurements, the measurements can hardly be used for the calibration of the modelling.

4.2.4. General discussion

As shown above, all three analytical models are able to describe the decreasing trend of strength along the tested specimen size range. Assuming that the Weibull modulus $m = 6$ for cement paste under such one-sided splitting test, the fitting results of case 2 in Table 7, case 3 in Table 8 and case 4 in Table 9 are plotted together in Fig. 12 for comparison. In the range of tested specimen sizes, Bazant's ESSET is capable to shift to any point apart from the linear line (Weibull size effect), while MFSL gradually grows from a slope of -0.5 at small-scale asymptote towards a horizontal line for the large-scale specimen. It is interesting to mention that both the Weibull size effect model and Carpinteri's MFSL behave linear in the small-scale asymptote with a slope of -0.5 . Such slope at small-scale asymptote is inherent to the MFSL. The agreement between the Weibull size effect and MFSL might prove that the role of microstructural disorder and of self-similar features dominate the damage and fracturing processes of cement paste at the micro-scale [56]. However, Bazant's ESSET gives a constant strength for small specimen sizes (plastic limit). Even with the unprecedented size range of experimental data, such plastic limit could not be captured in current work. For strength measurements of



(a)



(b)

Fig. 13. Simulated load-displacement curve of the digital specimens with size of (a) 0.1 mm and (b) 5 mm.

specimens smaller than $10 \mu\text{m}$, it is possible to use a focused ion beam for specimen preparation and the nanoindenter for mechanical testing [9,10]. However, when the specimens are so small, the measured strength is not representative of cement paste anymore, as the material might only contain a single cement phase (for example, Calcium-Silicate-Hydrate or Portlandite). Thus, the small-size asymptote can never be measured experimentally for cement paste. In turn, the attention might be put on validation of these size effect models at large-scale (structure size scale), which is more of practical importance. As shown in Fig. 12, a different trend is found between the ESSET and MFSL at this size range. Specifically, Bazant's ESSET (equation (8)) turns to be parallel with the Weibull size effect in the large-scale asymptote with a slope value -0.5 in this case, because the parameter D_b is close to 0. Whereas Carpinteri's MFSL shifts to a horizontal line. Large sized experiments should therefore be carried out for validation. The challenges related with such large-scale experiments are the demands of the testing instruments which can operate the big size specimen and have enough load capacity, and the specimen preparation which might make it impossible use cement paste as a material because of the shrinkage and eigenstress which will develop in large specimens during the hydration

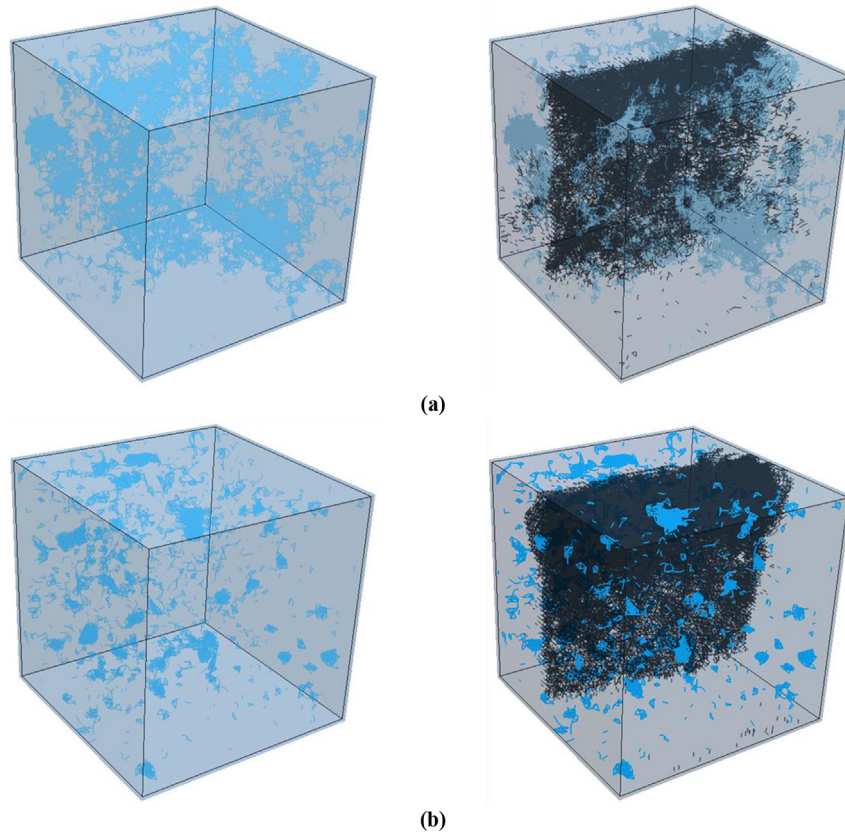


Fig. 14. Spatial distribution of pores (left) and fracture pattern (right) of the digital specimens with size of (a) 0.1 mm and (b) 5 mm (blue –pore, black-crack). (For interpretation of the references to colour in this figure legend, the reader is referred to the Web version of this article.)

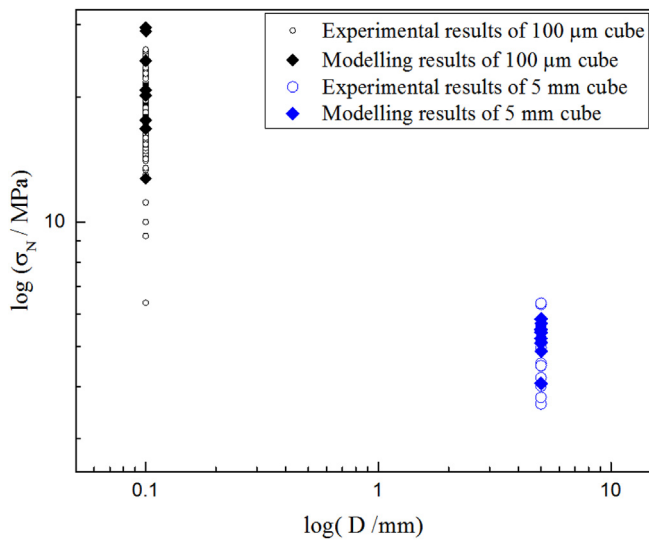


Fig. 15. Comparison between the modelling results and experimental results in terms of the nominal splitting strength.

process.

4.3. Modelling results and discussion

Using the multi-scale modelling strategy described in Section 3.2, the one-sided splitting test was simulated on specimens of two sizes: 0.1 mm and 5 mm. As the simulated mechanical behaviour of 0.1 mm has been validated in Ref. [14] by comparing both the load-displacement response and crack pattern with experimental data, herein the

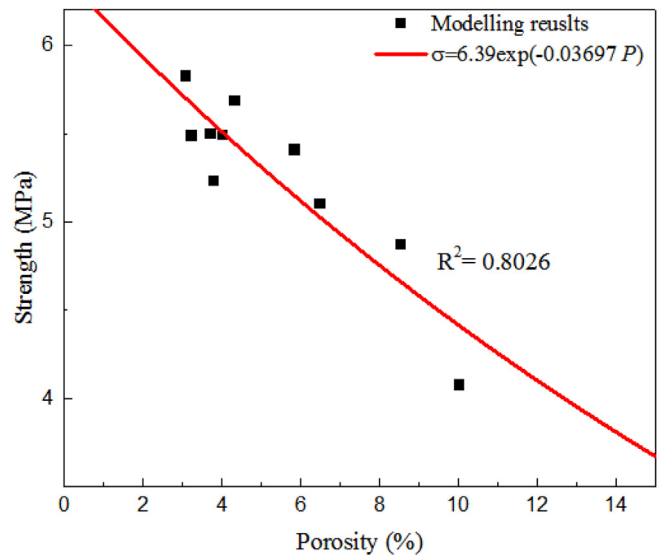


Fig. 16. Relationship between nominal splitting strength and population of meso-pore for the 5 mm specimens.

focus is on the different fracture response of specimens of different sizes. Simulated load-displacement diagrams of each size family are plotted in Fig. 13. For each size family, 10 specimens were simulated to show the scatter. Compared with the 0.1 mm specimens, a relatively brittle post peak behaviour is found for the 5 mm specimens (note again that, due to the limitations of the tests performed, post-peak was not measured experimentally). This is mainly because of the different material structures. For 0.1 mm specimens, a more tortuous and distributed crack pattern is found (see Fig. 14), due to presence of the

capillary pores and anhydrous cement particles. More specifically, on one hand, capillary pores introduce stress concentrations and micro cracks initialize in their vicinity. On the other hand, the anhydrous cement particles work as stiff inclusions in the matrix which disturb the crack pattern propagation path when crack localization starts. In the 5 mm specimens, the capillary pores and anhydrous cement particles are homogenised as the cement matrix, although the distributed cracks can be found due to the presence of large capillary pores or entrapped air voids, the ‘stiff inclusion effect’ disappears as the particle size is only visualized within the micro length scale.

In order to assess whether the proposed microstructure-informed lattice model is capable of accurately predicting the strength of cement paste at multiple scales, the nominal splitting strength was calculated from the peak load using Equation (2), and compared with experimental results (see Fig. 15). The calculated average splitting strengths are 22.00 MPa for 0.1 mm size specimen and 5.27 MPa for the 5 mm specimen. The fluctuation is captured by the modelling strategy: a CoV of 0.095 is found for 5 mm size specimen, while a higher CoV value (0.260) is obtained for 0.1 mm size specimen. Note that the simulation covers a wide size range of 1: 50. Although smaller than the tested size range, it is still 6 times larger than the simulated range in previous studies [24,25]. It is known that with a constant resolution and increasing the material size in the 3D discrete model, the computational demands are increased as a power law and thus the investigated size range was limited. A multi-scale modelling strategy as proposed herein is capable of enlarging the prediction size over several length scales to have more insight into the influence of microstructural features on the material's fracture behaviours.

As shown by the authors [31,33], such model offers further insight into the relation between the microstructural features and its corresponding mechanical properties. For example, the influence of the population of micro-scale pores on the micromechanical properties has been previously studied [14,31,33]. In the current study, the influence of the micro-pores is taken indirectly in simulations of specimens as the homogenised cement paste matrix. The relation between the meso-scale porosity ($\geq 100 \mu\text{m}$) and simulated strength is plotted in Fig. 16. Clearly, the nominal splitting strength decreases exponentially with increasing population of meso-scale pores. The scatter can be attributed to the variation of pore size distribution and its spatial distribution in each single specimen. Both factors are known to play an important role in the fracture process [57,58]. Based on the modelling approach proposed herein, further studies could be carried out using advanced image analysis methods and pore structure characterization approaches (e.g., Ref. [30]) to have more quantitative investigation on the influence of the multi-scale pore structures on the fracture process.

5. Conclusions

The experimental basis for the size effect (size range: 0.1–40 mm) study has been successfully extended by the present work. Based on the unprecedented size range of strength measurements, existing analytical models for size effect are critically examined. A microstructure-informed discrete model has been used to simulate the fracture of specimens at both micro and meso-scales. Based on the presented results, the following conclusions can be drawn:

- It is confirmed by the experimental measurements that the splitting tensile strength of cement paste at micro-scale is significantly higher than the one measured from the laboratory (centimetre sized) scale. Together with the measured average strength, the scatter (CoV) of the measurements decreases with the specimen size increasing.
- The two-parameter Weibull analysis reveals that, on one hand, regarding the same fracture strength (below 30 MPa), the smaller specimen has a lower fracture probability, while, on the other hand, for the same fracture probability, the smaller specimen tends to yield a higher strength.
- Although all examined analytical models can be fitted with a high determination coefficient, special attention should be given to the physical meaning behind these empirical parameters. Controversial trends were found in both small and large size asymptotes for multifractal scaling law and energetic-statistical size effect theory, which could not be validated nor disproved by the experiments performed herein.
- The lattice model is able to predict strengths that are in good accordance with the experimental measurements for both 0.1 mm and 5 mm specimens as well as the fluctuations. With the multi-scale modelling strategy adopted herein, the size range of microstructure-informed 3D discrete model on strength prediction is significantly enlarged.
- Because of the presence of capillary pores and anhydrous cement particles, a higher degree of heterogeneity is observed in the model at the micro-scale. This results in a more tortuous and diffuse crack pattern as well as a more ductile post-peak behaviour.
- The current model can provide a link between the material structure and the predicted mechanical properties. An exponential equation is proposed to express the relationship between predicted strength and porosity that is explicitly presented in the model. The dispersion between the proposed empirical strength-porosity relationship and numerical modelling results can be attributed to the variation of pore size distribution and its spatial distribution in each single specimen. By combining more advanced image analysis methods and pore structure characterization approaches, the proposed modelling approach can offer insight into the relation between the pore structure and fracture properties of materials.

Acknowledgements

Hongzhi Zhang and Yading Xu would like to acknowledge the funding supported by China Scholarship Council under grant No.201506120067 and CSC No.201708110187, respectively. The authors would like to acknowledge Mr. Maiko van Leeuwen for his support in the mechanical tests and Mr. Arjan Thijssen for his assistance in ESEM work.

Appendix A. Supplementary data

Supplementary data to this article can be found online at <https://doi.org/10.1016/j.cemconcomp.2018.09.018>.

References

- [1] P. Chindaprasirt, C. Jaturapitakkul, T. Sinsiri, Effect of fly ash fineness on compressive strength and pore size of blended cement paste, *Cement Concr. Compos.* 27 (2005) 425–428.
- [2] P. Gu, J.J. Beaudoin, E.G. Quinn, R.E. Myers, Early strength development and hydration of ordinary Portland cement/calcium aluminate cement pastes, *Adv. Cement Base Mater.* 6 (1997) 53–58.
- [3] T.C. Powers, T.L. Brownyard, Studies of the physical properties of hardened Portland cement paste, *Journal Proceedings* (1946) 101–132.
- [4] P.J. Sandberg, F. Doncaster, On the mechanism of strength enhancement of cement paste and mortar with triisopropanolamine, *Cement Concr. Res.* 34 (2004) 973–976.
- [5] H. Ma, D. Hou, Y. Lu, Z. Li, Two-scale modeling of the capillary network in hydrated cement paste, *Construct. Build. Mater.* 64 (2014) 11–21.
- [6] Z.P. Bažant, Size effect, *Int. J. Solid Struct.* 37 (2000) 69–80.
- [7] J.G. Van Mier, *Concrete Fracture: a Multiscale Approach*, CRC press, 2012.
- [8] M.F. Pantano, H.D. Espinosa, L. Pagnotta, Mechanical characterization of materials at small length scales, *J. Mech. Sci. Technol.* 26 (2012) 545–561.
- [9] S.J. Chen, W.H. Duan, Z.J. Li, T.B. Sui, New approach for characterisation of mechanical properties of cement paste at micrometre scale, *Mater. Des.* 87 (2015) 992–995.
- [10] J. Němeček, V. Králík, V. Šmilauer, L. Polívka, A. Jäger, Tensile strength of hydrated cement paste phases assessed by micro-bending tests and nanoindentation, *Cement Concr. Compos.* 73 (2016) 164–173.
- [11] R. Shahrin, C.P. Bobko, Characterizing strength and failure of calcium silicate hydrate aggregates in cement paste under micropillar compression, *Journal of Nanomechanics and Micromechanics* 7 (2017) 06017002.
- [12] M.J. Pfeifenberger, M. Mangang, S. Wurster, J. Reiser, A. Hohenwarther, W. Pflieger,

- et al., The use of femtosecond laser ablation as a novel tool for rapid micro-mechanical sample preparation, *Mater. Des.* 121 (2017) 109–118.
- [13] B. Šavija, D. Liu, G. Smith, K.R. Hallam, E. Schlangen, P.E. Flewitt, Experimentally informed multi-scale modelling of mechanical properties of quasi-brittle nuclear graphite, *Eng. Fract. Mech.* 153 (2016) 360–377.
- [14] H. Zhang, B. Šavija, E. Schlangen, Combined experimental and numerical study on micro-cube indentation splitting test of cement paste, *Eng. Fract. Mech.* 199 (2018) 773–786.
- [15] H. Zhang, B. Šavija, S. Chaves Figueiredo, M. Lukovic, E. Schlangen, Microscale testing and modelling of cement paste as basis for multi-scale modelling, *Materials* 9 (2016) 907.
- [16] A. Carpinteri, B. Chiaia, Multifractal scaling laws in the breaking behaviour of disordered materials, *Chaos, Solit. Fractals* 8 (1997) 135–150.
- [17] A. Carpinteri, B. Chiaia, G. Ferro, Size effects on nominal tensile strength of concrete structures: multifractality of material ligaments and dimensional transition from order to disorder, *Mater. Struct.* 28 (1995) 311.
- [18] A. Carpinteri, B. Chiaia, P. Cornetti, S. Puzzi, Comments on “Is the cause of size effect on structural strength fractal or energetic-statistical?” by Bažant & Yavari [*Engng Fract Mech* 2005; 72: 1–31], *Eng. Fract. Mech.* 74 (2007) 2892–2896.
- [19] Z.P. Bažant, Size effect in blunt fracture: concrete, rock, metal, *J. Eng. Mech.* 110 (1984) 518–535.
- [20] Z.P. Bažant, M. Vořechovský, D. Novák, Asymptotic prediction of energetic-statistical size effect from deterministic finite-element solutions, *J. Eng. Mech.* 133 (2007) 153–162.
- [21] Z.P. Bažant, S.-D. Pang, Activation energy based extreme value statistics and size effect in brittle and quasibrittle fracture, *J. Mech. Phys. Solid.* 55 (2007) 91–131.
- [22] R. Ince, A. Arslan, B. Karihaloo, Lattice modelling of size effect in concrete strength, *Eng. Fract. Mech.* 70 (2003) 2307–2320.
- [23] J. Van Mier, M. Van Vliet, Influence of microstructure of concrete on size/scale effects in tensile fracture, *Eng. Fract. Mech.* 70 (2003) 2281–2306.
- [24] H.-K. Man, J. Van Mier, Damage distribution and size effect in numerical concrete from lattice analyses, *Cement Concr. Compos.* 33 (2011) 867–880.
- [25] H.-K. Man, J.G. van Mier, Size effect on strength and fracture energy for numerical concrete with realistic aggregate shapes, *Int. J. Fract.* 154 (2008) 61–72.
- [26] E. Schlangen, E. Garboczi, Fracture simulations of concrete using lattice models: computational aspects, *Eng. Fract. Mech.* 57 (1997) 319–332.
- [27] Z. Qian, Multiscale Modeling of Fracture Processes in Cementitious Materials, [Ph.D. Thesis] Delft University of Technology, Delft, The Netherlands, 2012.
- [28] B. Šavija, H. Zhang, E. Schlangen, Influence of microencapsulated phase change material (PCM) addition on (micro) mechanical properties of cement paste, *Materials* 10 (2017) 863.
- [29] M. Zhang, A.P. Jivkov, Micromechanical modelling of deformation and fracture of hydrating cement paste using X-ray computed tomography characterisation, *Compos. B Eng.* 88 (2016) 64–72.
- [30] T.-S. Han, X. Zhang, J.-S. Kim, S.-Y. Chung, J.-H. Lim, C. Linder, Area of lineal-path function for describing the pore microstructures of cement paste and their relations to the mechanical properties simulated from μ -CT microstructures, *Cement Concr. Compos.* 89 (2018) 1–17.
- [31] H. Zhang, B. Šavija, E. Schlangen, Towards understanding stochastic fracture performance of cement paste at micro length scale based on numerical simulation, *Construct. Build. Mater.* 183 (2018) 189–201.
- [32] E. Gallucci, K. Scrivener, A. Groso, M. Stapanoni, G. Margaritondo, 3D experimental investigation of the microstructure of cement pastes using synchrotron X-ray microtomography (μ CT), *Cement Concr. Res.* 37 (2007) 360–368.
- [33] H. Zhang, B. Šavija, S.C. Figueiredo, E. Schlangen, Experimentally validated multi-scale modelling scheme of deformation and fracture of cement paste, *Cement Concr. Res.* 102 (2017) 175–186.
- [34] A. Delaplace, G. Pijaudier-Cabot, S. Roux, Progressive damage in discrete models and consequences on continuum modelling, *J. Mech. Phys. Solid.* 44 (1996) 99–136.
- [35] M. Yip, J. Mohle, J. Bolander, Automated modeling of three-dimensional structural components using irregular lattices, *Comput. Aided Civ. Infrastruct. Eng.* 20 (2005) 393–407.
- [36] G. Lilliu, J.G. van Mier, 3D lattice type fracture model for concrete, *Eng. Fract. Mech.* 70 (2003) 927–941.
- [37] B. Šavija, J. Pacheco, E. Schlangen, Lattice modeling of chloride diffusion in sound and cracked concrete, *Cement Concr. Compos.* 42 (2013) 30–40.
- [38] G. Lilliu, 3D Analysis of Fracture Processes in Concrete, Delft University of Technology, Delft, The Netherlands, 2007.
- [39] I. Gitman, H. Askes, L. Sluys, Representative volume: existence and size determination, *Eng. Fract. Mech.* 74 (2007) 2518–2534.
- [40] Z. Qian, E. Schlangen, G. Ye, K. van Breugel, Modeling framework for fracture in multiscale cement-based material structures, *Materials* 10 (2017) 587.
- [41] Z. Qian, E. Schlangen, G. Ye, K. Van Breugel, Prediction of mechanical properties of cement paste at microscale, *Mater. Construcción* 60 (2010) 7–18.
- [42] C. Hu, Z. Li, Micromechanical investigation of Portland cement paste, *Construct. Build. Mater.* 71 (2014) 44–52.
- [43] M. Hlobil, V. Šmilauer, G. Chanvillard, Micromechanical multiscale fracture model for compressive strength of blended cement pastes, *Cement Concr. Res.* 83 (2016) 188–202.
- [44] D. Liu, K. Mingard, O.T. Lord, P. Flewitt, On the damage and fracture of nuclear graphite at multiple length-scales, *JNuM* 493 (2017) 246–254.
- [45] J.B. Wachtman, W.R. Cannon, M.J. Matthewson, *Mechanical Properties of Ceramics*, John Wiley & Sons, 2009.
- [46] J.B. Quinn, G.D. Quinn, A practical and systematic review of Weibull statistics for reporting strengths of dental materials, *Dent. Mater.* 26 (2010) 135–147.
- [47] D.R. Thoman, L.J. Bain, C.E. Antle, Inferences on the parameters of the Weibull distribution, *Technometrics* 11 (1969) 445–460.
- [48] P. Milella, N. Bonora, On the dependence of the Weibull exponent on geometry and loading conditions and its implications on the fracture toughness probability curve using a local approach criterion, *Int. J. Fract.* 104 (2000) 71–87.
- [49] W. Weibull, A statistical distribution function of wide applicability, *J. Appl. Mech.* 18 (1951) 290–293.
- [50] Z. Bazant, Y. Xi, Statistical size effect in quasi-brittle structures: II, Nonlocal theory, *J Eng Mech.* 117 (1991) 2623–2640.
- [51] J.J. Moré, D.C. Sorensen, Computing a trust region step, *SIAM J. Sci. Stat. Comput.* 4 (1983) 553–572.
- [52] B. Zech, F. Wittmann, Part II Probabilistic approach to describe the behaviour of materials, *NuEnD* 48 (1978) 575–584.
- [53] M.R. Van Vliet, J.G. Van Mier, Experimental investigation of size effect in concrete and sandstone under uniaxial tension, *Eng. Fract. Mech.* 65 (2000) 165–188.
- [54] Z.P. Bažant, A. Yavari, Is the cause of size effect on structural strength fractal or energetic-statistical? *Eng. Fract. Mech.* 72 (2005) 1–31.
- [55] Z.P. Bažant, S.D. Pang, M. Vořechovský, D. Novák, Energetic-statistical size effect simulated by SFEM with stratified sampling and crack band model, *IJNME* 71 (2007) 1297–1320.
- [56] A. Carpinteri, S. Puzzi, *Fractals, Statistics and Size-scale Effects on Concrete Strength, Fracture Mechanics of Concrete Structures*, 2007, pp. 31–37.
- [57] D. Liu, B. Šavija, G.E. Smith, P.E. Flewitt, T. Lowe, E. Schlangen, Towards understanding the influence of porosity on mechanical and fracture behaviour of quasi-brittle materials: experiments and modelling, *Int. J. Fract.* (2017) 1–16.
- [58] H. Chandler, I. Merchant, R. Henderson, D. Macphee, Enhanced crack-bridging by unbonded inclusions in a brittle matrix, *J. Eur. Ceram. Soc.* 22 (2002) 129–134.